Optical and Photophysical Studies on Porphyrin Doped TiO_2 Matrixes

Teresa M. R. Viseu,* Graham Hungerford, and Maria Isabel C. Ferreira

Centro de Física, Universidade do Minho, 4710-057 Braga, Portugal

Received: August 10, 2001; In Final Form: October 30, 2001

The extinction coefficient, $k(E)$, and refractive index, $n(E)$, of zinc *meso*-tetra porphyrin (ZnP) when incorporated into nanoporous titania were measured in the range 1.7−4.2 eV, by using a method that accounts for both the microstructure and morphology of the semiconductor matrix. Optical and fluorescence spectra reveal the presence of a specific interaction between the porphyrin and TiO_2 whereby ZnP becomes anchored onto the surface of porous titania in monomeric and as aggregated forms. Radiative decays and fluorescence quantum yields were determined for the two forms of ZnP. The work also included optical and fluorescence studies of ZnP bound to poly(4-vinylpyridine) (PVP). In this case formation of a ground-state complex, ZnP−PVP, prevents aggregation of the porphyrin. The complex is fluorescent, with two distinct radiative decays determined by the micropolarities of the PVP copolymer.

1. Introduction

In the field of solar energy conversion the so-called Grätzel cell[1] has prompted a large number of contributions on dye sensitization of TiO_2.[2] Important progress on the role of the semiconductor TiO_2 was achieved either by means of theoretical studies[3] or by the vast experimental data that have been published, such as the contributions of Durrant et al.[4] and Koehorst et al.[5] It is a well-known fact that the microporous morphology of TiO_2 is an important feature in the Grätzel cell inasmuch as it provides a large surface area for an appropriate dye−semiconductor interaction.[6] This interaction is determinant to the high yield of electron injection into titania and thus controls the overall efficiency of the solar cell. The yield of solar light absorption of the cell is another key factor on the overall conversion efficiency of such devices.[7] Porphyrins are very efficient light absorbers, particularly in the range 400−700 nm,[8] and therefore good candidates as photosensitizers.

The possibility of developing new solar cells based on hybrid systems where the dye is a porphyrin[9,10] has prompted us to study the photophysical and spectroscopic properties of zinc *meso*-tetra porphyrin (ZnP) when incorporated in TiO_2 matrixes. Previous work[11,12] has shown that the spectroscopic behavior of porphyrins and phthalocyanines is significantly influenced by the microenvironment within the sol−gel-derived matrix pores.

In this work we report on the steady state and time-resolved fluorescence of ZnP when incorporated into TiO_2 matrixes produced by the sol−gel method and by reactive magnetron sputtering. The extinction and absorption coefficients of these hybrid materials were also determined by considering an effective medium theory that takes into account the microstructure and morphology of the host matrixes. These studies have provided information on the specific interaction between the porphyrin and the semiconductor matrix. Such interaction will determine to a significant extent not only the absorption efficiency of solar radiation of these materials but also the efficiency of dye-sensitized charge-transfer processes. The presence and the role of aggregated forms of ZnP were also investigated. These studies were further extended to another hybrid system where the porphyrin (ZnP) and poly(4-vinylpyridine) (PVP) were deposited onto the semiconductor matrixes. The photophysics of the ZnP−PVP system has provided relevant information on the radiative decay kinetics of ZnP fluorescence in the presence of this polymeric environment.

2. Experimental Section

Zinc *meso*-tetra porphyrin dihydrochloride (ZnP) was purchased from Porphyrin Products Inc. and used without further purification. Poly(4-vinylpyridine-*co*-styrene), styrene content 10%, (PVP), from Aldrich, was used as supplied. Stock solutions of each porphyrin in methanol were prepared and further used to dope the TiO_2 matrixes. These matrixes were prepared either by the sol−gel technique, as previously reported[11] or by reactive sputtering. In the first case film samples of titania, TiO_2(sg), were cast at the onset of the full gelation process, by means of a homemade dipping apparatus. The films were allowed to dry at room temperature for 2 weeks. Sputtered films, TiO_2(sp), were prepared by reactive magnetron sputtering in a commercial Alcatel System, model SCM 650, under preparation conditions already described.[13] All samples were produced as films deposited onto glass slides. The porphyrin was then incorporated by dipping each TiO_2 sample in the stock solution of porphyrin. After dipping, each sample was allowed to dry for several days and then cleaned with a soft tissue. After this period no further changes were found in the transmittance and fluorescence spectra of the samples in the range 250−2200 and 550−800 nm, respectively.

Doping of the TiO_2 matrixes was performed only after the structure and the optical parameters of nanostructured anatase were determined. The structure of the TiO_2 matrixes was examined by X-ray diffractometry (XRD) using a Philips PW1710 diffractometer. The following optical parameters, refractive index, extinction coefficient, and thickness, were obtained by detailed analysis of the transmittance spectra. Transmittance spectra were measured on a Shimadzu UV-3101 PC from 250 to 2200 nm.

Fluorescence and excitation spectra of the doped films were recorded on a Spex Fluorolog in the front face configuration in

* Corresponding author. E-mail: tviseu@fisica.uminho.pt. Fax: 351-253 678 981.

10.1021/jp013134n CCC: $22.00
Published on Web 02/01/2002

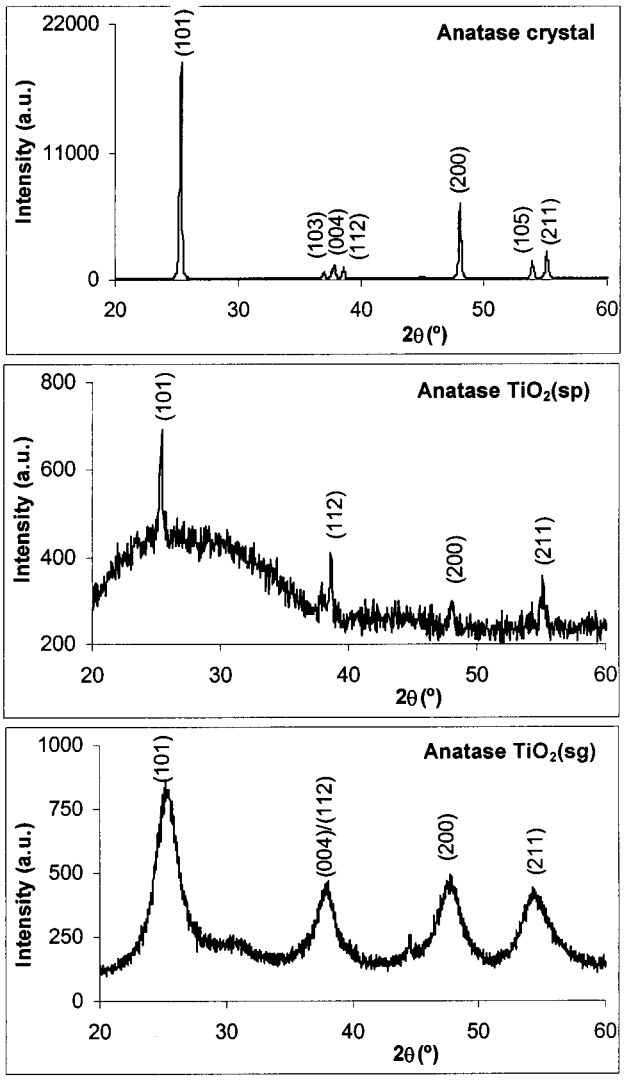

Figure 1. X-ray diffraction spectra of crystalline anatase and TiO_2 thin films prepared by reactive sputtering and by the sol−gel technique.

order to minimize any self-absorption effects. Fluorescence quantum yields, ϕ_F, were obtained relative to a dry sample of rhodamine 6G incorporated in a SiO_2 matrix.[14] The optically dilute method was used[15] and corrections were made by considering the relative intensity of the Xe lamp at the excitation wavelengths, the optical density, and the effective refractive index of each medium. Fluorescence lifetimes were measured by means of a single-photon counting apparatus equipped with a hydrogen-filled coaxial flash lamp. The required excitation wavelength (maximum of the Soret band) was selected via a monochromator. Cutoff filters were used to select the emission signal ($\lambda_{emission} > 550$ nm), which was then detected using a Hamamatsu R-2949 side-window photomultiplier, except for the ZnP-MeOH measurement where a Philips XP 2020Q was employed. Data analysis was performed using software provided by IBH Consultants Ltd. Errors are given as three standard deviations, and the contribution of each fluorescent component is expressed as a relative preexponential factor. All measurements were performed at room temperature.

3. Matrix Characterization

X-ray diffractometry of all titania samples, in the high angle configuration geometry, show diffraction peaks that can be ascribed to the anatase variety of TiO_2, as shown in Figure 1, where the X-ray diffractogram of crystalline anatase is also shown for comparison. The wider diffraction peaks found for sol−gel-derived anatase indicate a shorter coherence length for these samples as compared with the samples produced by sputtering. For sol−gel-derived anatase the coherence length was found to be on the order of 3 nm, by applying the treatment proposed by Langford[16] to the measured diffraction peaks. From recent studies[17] it was found that the characteristic dimension of sputtered anatase nanocrystals, prepared under conditions identical to those in the present work, is on the order of 5−8 nm. Moreover, the same study[17] has shown that the characteristic size of the voids in the sputtered films is on the order of 2 nm, thus confirming that under these experimental conditions it is possible to prepare nanoporous anatase films where the average void dimension allows the doping by encapsulated porphyrin molecules within the pores. In fact, the principal radii of the porphinato skeleton of a metalloporphyrin are in the range 0.31−0.35 nm,[18] thus significantly smaller than the average pore size of the titania matrixes.

The optical constants of each nondoped matrix were determined from the detailed analysis of the transmittance spectra in the range 250−2200 nm, according to the Abelès matricial method,[19] which is particularly suitable to study multilayered materials. In fact, the relationship between the electric (**E**) and magnetic (**H**) fields in the air/film F_1 interface **(I)** and the film F_N/substrate interface **(II)** in a set of N optical layers is

$$\begin{bmatrix} \mathbf{E}_I \\ \mathbf{H}_I \end{bmatrix} = \mathbf{M} \begin{bmatrix} \mathbf{E}_{II} \\ \mathbf{H}_{II} \end{bmatrix}$$

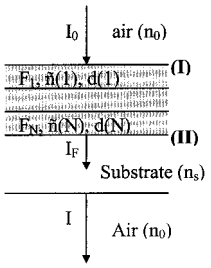

where **M** is the characteristic matrix of the multilayered film, and therefore,

$$\mathbf{M} = \prod_{j=1}^{N} \mathbf{M}_j = \mathbf{M}_1 \mathbf{M}_2 .... \mathbf{M}_N$$

Each $\mathbf{M}_j$ matrix is of type

$$\mathbf{M}_j = \begin{bmatrix} \cos\delta & i\dfrac{\sin\delta}{\tilde{n}} \\ i\tilde{n}\sin\delta & \cos\delta \end{bmatrix}$$

where $\delta = (2\pi/\lambda)\tilde{n}d$ and $\tilde{n} = \tilde{n} - ik$.

The transmittance of a multilayered film is

$$T = \frac{T_S T_F}{1 - R_S R_F} \tag{1}$$

where T_S and R_S are the substrate transmittance and reflectance, and T_F and R_F are the film transmittance and reflectance.

The behavior of the refractive index, $\tilde{n}$, of each layer was investigated by means of the unified treatment of Forouhi and Bloomer[20] applied to the optical range correspondent to the interband region of a solid, either crystalline or disordered. In the general case of the occurrence of several distinct interband

transitions, $k(E)$ becomes

$$k(E) = \left[\sum_i \frac{A_i}{(E - E_{0,i})^2 + \Gamma_i^2}\right](E - E_g)^2 \qquad (2)$$

where $E_{0,i}$ is the energy correspondent to a maximum of the probability transition (k maximum), E_g is the optical energy band gap, i.e., the energy at the onset of the fundamental interband absorption edge, andΓ_i is related to the width of absorption band i. Using the Kramers−Kronig relations, $n(E)$ is obtained analytically from $k(E)$:

$$n(E) = n(\infty) + \sum_i \frac{\rho_i(E - E_{0,i}) + \chi_i}{(E - E_{0,i})^2 + \Gamma_i^2} \qquad (3)$$

where

$$\rho_i = \frac{A_i}{\Gamma_i}(\Gamma_i^2 - (E_{0,i} - E_g)^2)$$

$$\chi_i = 2A_i\Gamma_i(E_{0,i} - E_g)$$

From the dispersion relations (2) and (3) and eq 1, simulated transmittance curves (T_{calc}) can be obtained. These curves are fitted to the measured ones (T_{exp}) and the best values of thickness, d, $n(E)$, and $k(E)$ of each layer thus obtained.

The quality of each fit is monitored by the residues, φ, defined as

$$\varphi = \left(\frac{\sum(T_{exp} - T_{calc})^2}{\sum(T_{exp})^2}\right)^{1/2}$$

According to this method it was found that all TiO_2 matrixes were optically equivalent to a single layer of nanoporous anatase. The void fraction of each film, $f(v)$, was determined by considering the measured effective refractive index as the result of multiple light scattering events at the pore−titania interfaces, in agreement with the theory developed by Webman et al.[21] Despite TiO_2 nanoporous morphology, light scattering in the 400−700 nm is negligible, as shown in Figure 2, where the transmittance of titania films confirms the high transparency of these films.[22] Figure 2 shows the best transmittance fits and the relevant fitting parameters obtained for TiO_2(sp) and TiO_2(sg) films. The lower effective refractive index of TiO_2(sg) as compared with TiO_2(sp), shown in the inset of Figure 2, is because of the higher void content. In this way the semiconducting matrixes as prepared provide not only an active support for the charge-transfer processes, as has been found by Grätzel and co-workers,[1] but also an adequate host to probe the photophysics of zinc *meso*-tetra porphyrin (ZnP) when encapsulated in TiO_2.

4. Optical and Fluorescence Spectra of the Porphyrin-Doped Matrixes

4.1. Optical Studies. The transmittance spectra of all doped films were measured in the range 250−2000 nm. Figures 3 and 4 show the best transmittance fits and the corresponding optical parameters, $k(\lambda)$ and $n(\lambda)$ for ZnP−TiO_2(sp) and ZnP−TiO_2(sg), respectively.

For energies lower than the optical gap of the semiconductor (λ > 350 nm) the Soret absorption band of the porphyrin is clearly discernible in the transmittance spectra. The optical

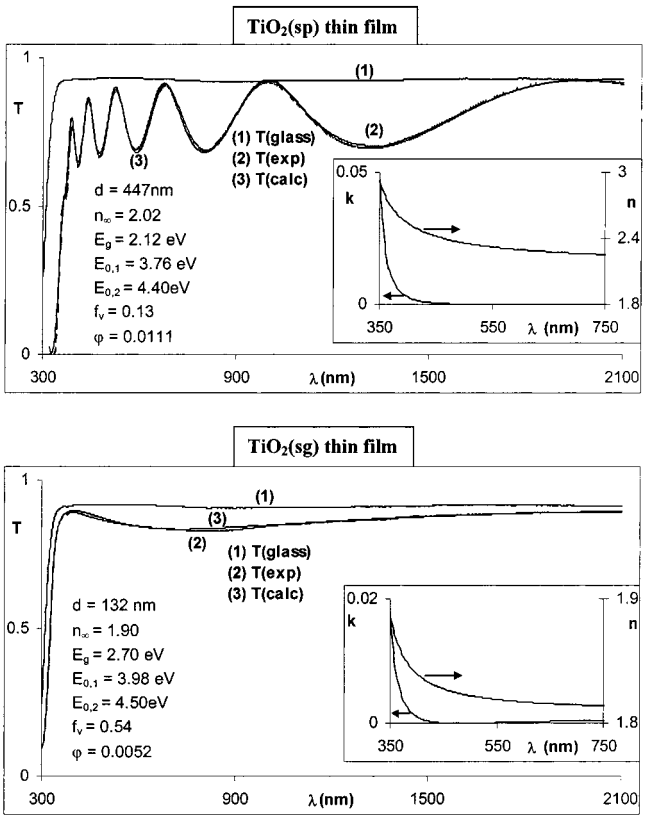

Figure 2. Measured and calculated transmittance for TiO_2(sp) and TiO_2(sg) thin films. The fit parameters are also shown along with the recovered $k(\lambda)$ and $n(\lambda)$ (inset).

dispersion attributed to ZnP in the 400−700 nm region was assumed to arise from electronic transitions between two localized (molecular) states, either $S_0 \rightarrow S_2$, for the Soret band or $S_0 \rightarrow S_1$ for the Q-bands. According to first-order perturbation theory, the extinction coefficient, $k(E)$, for the transition from state $|a\rangle$ to state $|b\rangle$ is given by[23,24]

$$k(E) = A\frac{\gamma}{(E_0 - E)^2 + \frac{\hbar^2\gamma^2}{4}}$$

where A contains the transition moment dipole and $E_0 = E_b - E_a$ is the resonant energy. Under these assumptions the complex dielectric constant of ZnP is given by the following equation, when in the presence of several resonant energies:

$$\tilde{\epsilon}(E) = B + \sum_j\left[\frac{C_j}{({E_{0,j}}^2 - E^2) - i\hbar\gamma_j E}\right] \qquad (4)$$

where $E_{0,j}$ corresponds to a maximum of the probability transition (k maximum). The dielectric constant is related to the refractive index, $\tilde{n}(E)$, according to

$$\tilde{\epsilon}(E) = \epsilon_r + i\epsilon_i = (n^2 - k^2) + i2nk$$

The absorption coefficient of ZnP in each sample can be obtained from the general expression

$$\alpha(E) = \frac{2Ek(E)}{\hbar c}$$

The values of $k(E)$, $n(E)$, $E_{0,i}$, and γ_i of ZnP in each film and the corresponding volumic fraction of porphyrin, f_{ZnP}, were

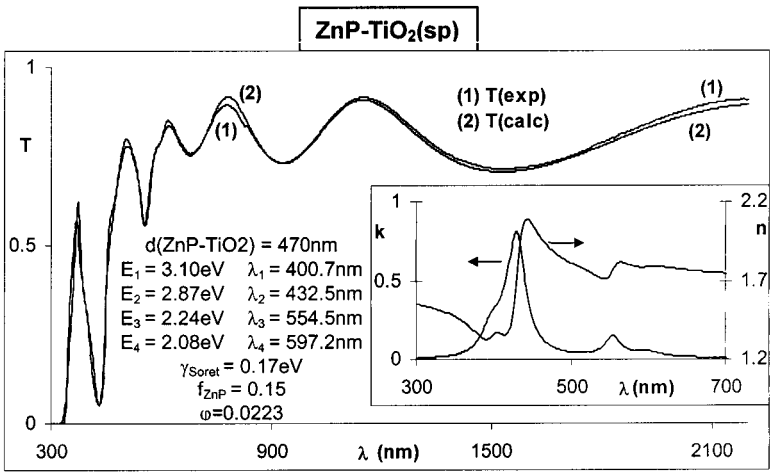

Figure 3. Measured and calculated transmittance spectra for the ZnP−TiO_2(sp) thin film. The fit parameters are also shown along with the recovered $k(\lambda)$ and $n(\lambda)$ for ZnP (inset).

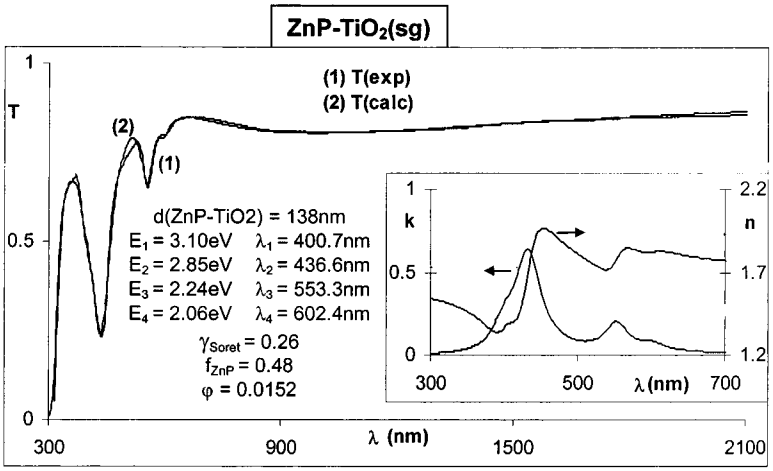

Figure 4. Measured and calculated transmittance spectra for the ZnP−TiO_2(sg) thin film. The fit parameters are also shown along with the recovered $k(\lambda)$ and $n(\lambda)$ for ZnP (inset).

TABLE 1: Relevant Data Obtained from the Analysis of the Transmittance Spectra of ZnP and ZnP−PVP Systems, as Thin Films and in Methanolic Solutions

sample	λ_{Soret} (nm)	λ_{Q_β} (nm)	λ_{Q_α} (nm)	I_{Q_α}/I_{Q_β}	γ_{Soret} (eV)
ZnP−TiO_2(sp)	432.5	554.5	597.2	0.39	0.17
ZnP−TiO_2(sg)	436.6	553.3	602.4	0.42	0.26
ZnP−PVP/TiO_2(sp)	433.6	565.2			0.062
ZnP−PVP/glass	433.5	564.6	605.1	0.60	0.058
ZnP (MeOH)	421.2	555.3	595.8	0.37	0.054
ZnP−PVP (MeOH)	428.2	562.0	603.0	0.60	0.062

obtained from the best fits between the transmittance curves simulated according to (4), T_{calc}, and the measured curves, T_{exp}, in the effective medium formalism.[21]

It was found that ZnP−TiO_2(sp) and ZnP−TiO_2(sg) systems were optically homogeneous and therefore considered to be one-layer films where ZnP is incorporated into nanoporous anatase the optical constants of which have been previously determined as described in section 3. $k(\lambda)$ spectra presented in the insets of Figures 3 and 4 show that the main features of the molecular absorption bands of the porphyrin are also present in the ZnP−TiO_2 systems. The maximum of the Soret band occurs at 432.5 and 436.6 nm for ZnP−TiO_2(sp) and ZnP−TiO_2(sg), respectively, therefore red shifted as compared with ZnP in methanol (λ_{Soret} = 421.2 nm, as can be seen in Table 1). The Q(1,0) band is slightly blue shifted in both films as compared with the same band in methanol, whereas the Q(0,0) band is slightly red-shifted. Moreover, the relative intensities of the two Q-bands, I_{Q_α}/I_{Q_β} (or $\epsilon_{Q_\alpha}/\epsilon_{Q_\beta}$), are on the order of 0.4 for both films such as for the solution in the polar solvent, methanol. These features suggest an interaction of ZnP with polar groups of the titania surfaces by means of an axial coordination to the central Zn atom of the porphyrin, in a fashion similar to what has been found by other authors[25−27] for ZnP in solution when in the presence of donor species such as N or O atoms. In fact, it is well-known that hydroxyl groups arising from tetrahedral and octahedral coordinations and also Ti_2O_3 are abundant on the surface of nanoporous titania.[28] The frequencies of the Q_α band and the ratio $\epsilon_{Q_\alpha}/\epsilon_{Q_\beta}$ found in this work are in agreement with the results reported by Valentine and Nappa[25] for ZnP-L and ZnP-X^- derivatives formed by axial coordination of L or X^- species to the central Zn atom of the porphyrin. Another important feature is the larger width of the Soret band, γ_{Soret}, in the ZnP−TiO_2 systems as compared with the corresponding values in solution (Table 1). This suggests the presence of aggregated ZnP on the titania surface, in agreement with previous work.[29] In fact, the axial coordination of Zn to O and OH surface groups of the matrix may induce an interaction between neighbor ZnP adsorbed/anchored molecules, thus displaying the spectroscopic behavior of an aggregate species. To elucidate this matter, we have examined in detail the absorbance in the Soret band of the ZnP−TiO_2(sp) film. This

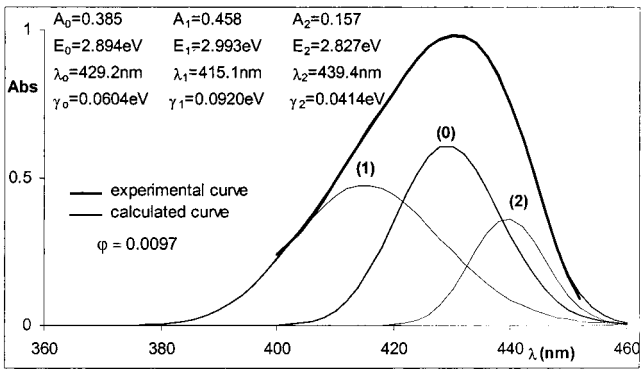

Figure 5. Decomposition of the measured Soret absorption band of the ZnP−TiO_2(sp) film, in the sum of three Gaussian curves, (0), (1), and (2).

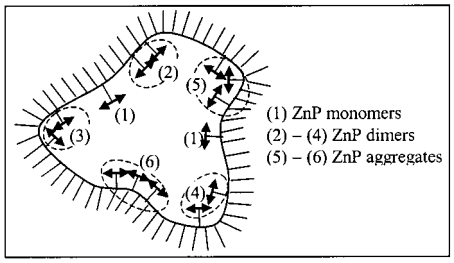

Figure 6. Schematic representation of a TiO_2 pore with incorporated ZnP molecules, showing several possible molecular orientations.

band was considered to be the sum of n Gaussian bands:

$$\mathrm{Abs}(E) = \sum_{i=1}^{n} \frac{A_i}{\gamma_i 2\pi} \mathrm{e}^{-(E-E_i)^2/2\gamma_i^2}$$

where Abs(E) is the total absorbance and A_i is the contribution of band i to the total spectrum. The best fit was obtained for $n = 3$, in the range 400−452 nm (3.10−2.75 eV), as shown in Figure 5. The fitting process was restricted to the range 400−452 nm in order to decrease the number of adjustable parameters. The corresponding fitting parameters are shown in the inset of Figure 5. The central band is ascribed to ZnP adsorbed onto titania as a monomer, whereas the two other bands are considered to originate from ZnP adsorbed in the form of aggregates, most probably with a diversity of molecular mutual orientations.[30] In fact, owing to the nonregular shape of the pores within the matrix, each porphyrin molecule may probe the presence of neighbor molecule(s) with different molecular orientations, as depicted in Figure 6. The width of the monomer absorption band is found to be 0.06 eV (Figure 5), a value comparable with the width of the Soret band of ZnP in methanol solution (Table 1, $\gamma_{\mathrm{Soret}} = 0.054$ eV). The larger value of γ_{Soret} for ZnP−TiO_2(sg) as compared with ZnP−TiO_2(sp) (Table 1) suggests higher chemical disorder at the TiO_2(sg) surfaces.

Addition of PVP to a solution of ZnP in methanol causes a red shift of ∼7 nm in the Soret band. The Q-bands become also red shifted by ∼7 nm and the ratio I_{Q_α}/I_{Q_β} is now 0.6, as shown in Table 1. It is known from previous studies[31,32] that ZnP and PVP form a ground-state complex when dissolved in methanol. In the presence of PVP the maximum of the Soret band of ZnP shifts from 421 nm in free porphyrin to 428 nm in bound ZnP, referred to as ZnP−PVP.[32] This complex is formed by axial coordination of one pyridine group of PVP to the Zn atom of the porphyrin, in agreement with other authors.[33,34]

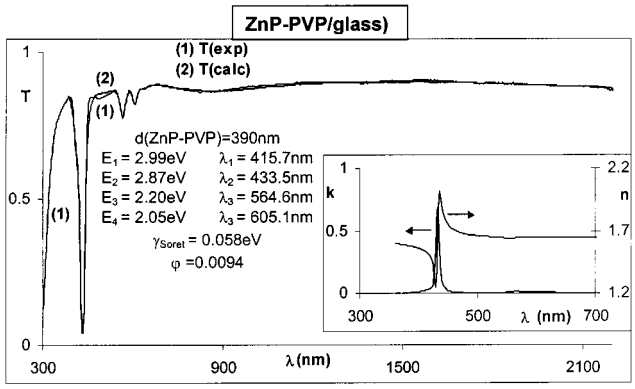

Figure 7. Measured and calculated transmittance spectra for the ZnP−PVP thin film. The fit parameters are also shown along with the recovered $k(\lambda)$ and $n(\lambda)$ (inset).

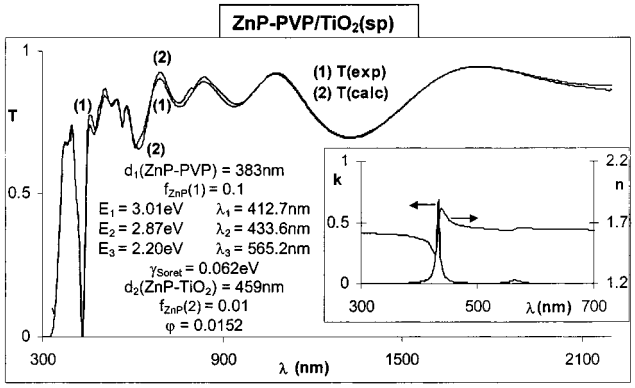

Figure 8. Measured and calculated transmittance spectra for the ZnP−PVP/TiO_2(sp) thin film. The fit parameters are also shown for layers 1 and 2 with the recovered $k(\lambda)$ and $n(\lambda)$ for layer 1 (inset).

The transmittance spectrum of a film containing ZnP and PVP (ZnP−PVP) deposited on a glass substrate is shown in Figure 7. $k(\lambda)$ and $n(\lambda)$ for this film, obtained from the best-fit parameters, are also shown in this figure. The maximum of the Soret band is now located at 433.5 nm, thus confirming the presence of ZnP bound to PVP. The relative intensities of the Q-bands, I_{Q_α}/I_{Q_β}, is on the order of 0.6, as found for ZnP−PVP in methanol. As can be seen in Table 1, the width of the Soret band for ZnP−PVP/glass ($\gamma_{\mathrm{Soret}} = 0.058$ eV), is now similar to the value found for ZnP in methanol ($\gamma_{\mathrm{Soret}} = 0.054$ eV), thus suggesting that in these systems the polymeric chains of PVP encage each porphyrin molecule, preventing interaction between ZnP molecules in the ground state.

When a film of TiO_2(sp) is doped with ZnP in the presence of PVP (ZnP−PVP/TiO_2(sp) film), the best fit, as shown in Figure 8, is obtained when T_{calc} is adjusted to a two-layered film such as

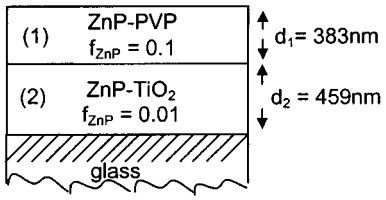

where the top layer has a thickness of $d_1 = 383$ nm and a high porphyrin content, $f_{\mathrm{ZnP}} = 0.1$, and the second layer possesses a much lower volumic fraction of ZnP ($f_{\mathrm{ZnP}} = 0.01$), its thickness being $d_2 = 459$ nm, obtained as explained in section 3. The top layer displays the typical behavior of ZnP embedded in PVP

TABLE 2: Data Obtained from Steady State and Time Resolved Fluorescence Measurements of ZnP and ZnP−PVP, in Films and Solutions

			ZnP−TiO_2(sp)		ZnP−PVP/glass		ZnP−PVP/TiO_2(sp)	
samples	ZnP/MeOH	ZnP−PVP/MeOH	monomer	aggregate	species I	species II	species I	species II
λ_{em}^{max} (nm)	601.5 (α)	607.5 (α)	601.3(α)	668.2	612.5	645.0	611.2	644.0
	654.2 (β)	659.5 (β)	653.5(β)	686.6	668.0	706.4	665.8	704.0
				715.6				
I_α/I_β	0.80	1.08	0.85		0.70	2.0	0.50	1.4
ϕ_F	0.028[a]	0.028[b]	0.028 ± 0.002		0.090 ± 0.004		0.089 ± 0.005	
			0.035	0.023				
τ_F[c] (ns)	1.90 ± 0.02	1.77 ± 0.02	2.10 ± 0.11 (0.46)[d]	0.77 ± 0.21 (0.53)[d]	1.08 ± 0.05 (0.42)[d]	0.60 ± 0.30 (0.57)[d]	0.94 ± 0.02 (0.35)[d]	0.34 ± 0.12 (0.64)[d]
χ^2	1.15	1.12	1.15		1.17		1.18	

[a] From ref 26. [b] From ref 32. [c] Time-resolved measurements were obtained exciting the samples in the maximum of the Soret band and detecting the emission for $\lambda > 550$ nm. [d] The preexponential factor.

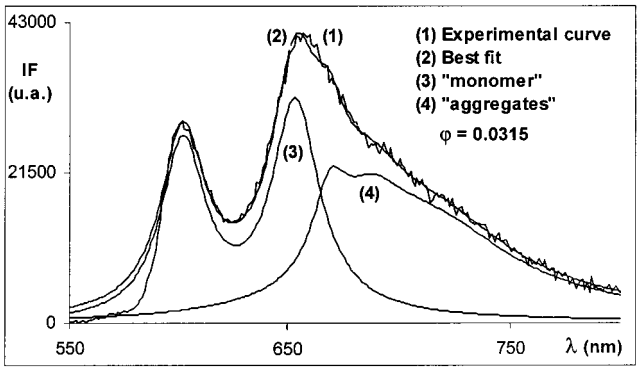

Figure 9. Measured and calculated fluorescence spectra of ZnP incorporated into the TiO_2 matrix, ZnP−TiO_2(sp). It is possible to distinguish two emissions, one ascribed to the monomer and the other to the "aggregates".

(inset of Figure 8) whereas the second (bottom) layer is characteristic of ZnP−TiO_2(sp). This behavior is interpreted as indicative that although most of the porphyrin is bound to the PVP chain and therefore unable to penetrate into the nanoporous structure of the semiconductor, some of the non-polymer-bound ZnP molecules in the doping solution may penetrate into the TiO_2 matrix. In fact, according to the equilibrium constant of the complex, $k \approx 88\ M^{-1}$,[32] about 3.6% of the total ZnP in the doping solution are not bound to the polymer. Table 1 summarizes the relevant data obtained from the analysis of the transmittance spectra of ZnP systems, with and without PVP, in methanol solutions and as thin films.

4.2. Emission Studies. Fluorescence of ZnP when incorporated into TiO_2, ZnP−TiO_2(sp), is shown in Figure 9, spectrum 1. The emission studies were performed on TiO_2(sp) matrixes since these display lower chemical disorder than TiO_2(sg), thus minimizing the ambiguities associated with the analysis of the fluorescence spectra and kinetics. All emission studies were performed on films with a very low dye content, i.e., OD < 0.1 at the Soret band peak. According to Figure 9, spectrum 1, emission from ZnP−TiO_2(sp) is characterized by two prominent bands at 602 and 655 nm. A broad shoulder also appears in the longer wavelength region. Due to the presence of aggregates, as stated in the former section, we have decomposed this spectrum by considering that the emission results from the superposition of several Lorentzian bands of variable widths. The best fit is shown in Figure 9, curve 2, where two distinct emissions could be found (curves 3 and 4). In the first one, ascribed to ZnP monomers, the Q(0,0) band occurs at 601.3 nm and the Q(0,1) band at 653.5 nm, in agreement with the corresponding band measured in methanolic solution, as can be seen in Table 2. The relative intensity of these bands, expressed as $I(F)_{Q_\alpha}/I(F)_{Q_\beta}$ is 0.85, a value somewhat higher than 0.80, the value found for ZnP in methanol, as shown in Table 2. This behavior corresponds with the values found for I_{Q_α}/I_{Q_β} in section 4.1 (Table 1) and therefore corroborates the concept of ZnP−matrix interaction through the axial coordination of the Zn central atom. The second spectrum (Figure 9, curve 4) is less structured, but three bands can still be resolved at 668.2, 686.6, and 715.6 nm. We ascribe this new red-shifted emission to the ZnP aggregates formed concomitantly with the ZnP−matrix interaction, as previously described in 4.1. This is in agreement with the work reported by Kemnitz and co-workers,[30] where absorption and emission studies of Rhodamine B adsorbed on quartz have provided evidence for the emission from dimers adsorbed on the silica surface. In fact, the theory of exciton splitting[35−37] predicts the existence of fluorescent or nonfluorescent dimers depending on the angle between the monomer transition dipole and the direction defined by the monomer geometrical centers of the molecular ensemble. Excitation spectra measured at 601 and 687 nm confirm that the 601 nm emission originates from the monomer, whereas the 687 nm emission originates from the red-shifted absorption band centered at ≈440 nm.

The global fluorescence quantum yield, Φ_F, of ZnP, obtained from spectrum 1 in Figure 9, is 0.028. To discriminate between the fluorescence quantum yield of ZnP as monomer, (ZnP)*, and as aggregate, $(ZnP)_n$*, we have considered the relative contribution of the monomer in this sample to be identical to the corresponding contribution in sample ZnP−TiO_2(sp) studied in section 4.1. We believe this approximation to be acceptable since the width of the Soret band in this sample, $\gamma_{Soret} = 0.16$ eV, is similar to the value 0.17 eV found for the sample analyzed in Figure 5. Using this approximation, we estimate that about 38.5% of all ZnP molecules are monomers and therefore we obtain the value 0.035 for the ZnP monomer quantum yield and 0.023 for the quantum yield of aggregated ZnP.

Figure 10b shows the fluorescence decay of ZnP−TiO_2(sp) in a nanosecond time scale. These data can be resolved into two major components, $\tau_1 = 0.77$ ns and $\tau_2 = 2.1$ ns. These results can be seen in Table 2. We assign the faster component to the aggregates and the longer lifetime to monomeric (isolated) ZnP, which is somewhat longer than that in methanol. This feature is in agreement with the higher rigidity to be expected from the adsorbed molecules, as compared with molecules in solution. Although the aggregate lifetime is smaller than the isolate ZnP lifetime, we admit that direct electron transfer from the first excited singlet of ZnP aggregates to the conduction band of TiO_2 is not a preponderant route for deactivation. In fact, electron transfer has been reported to be in the subnanosecond time scale, according to Durrant et al.[38] and Willig et

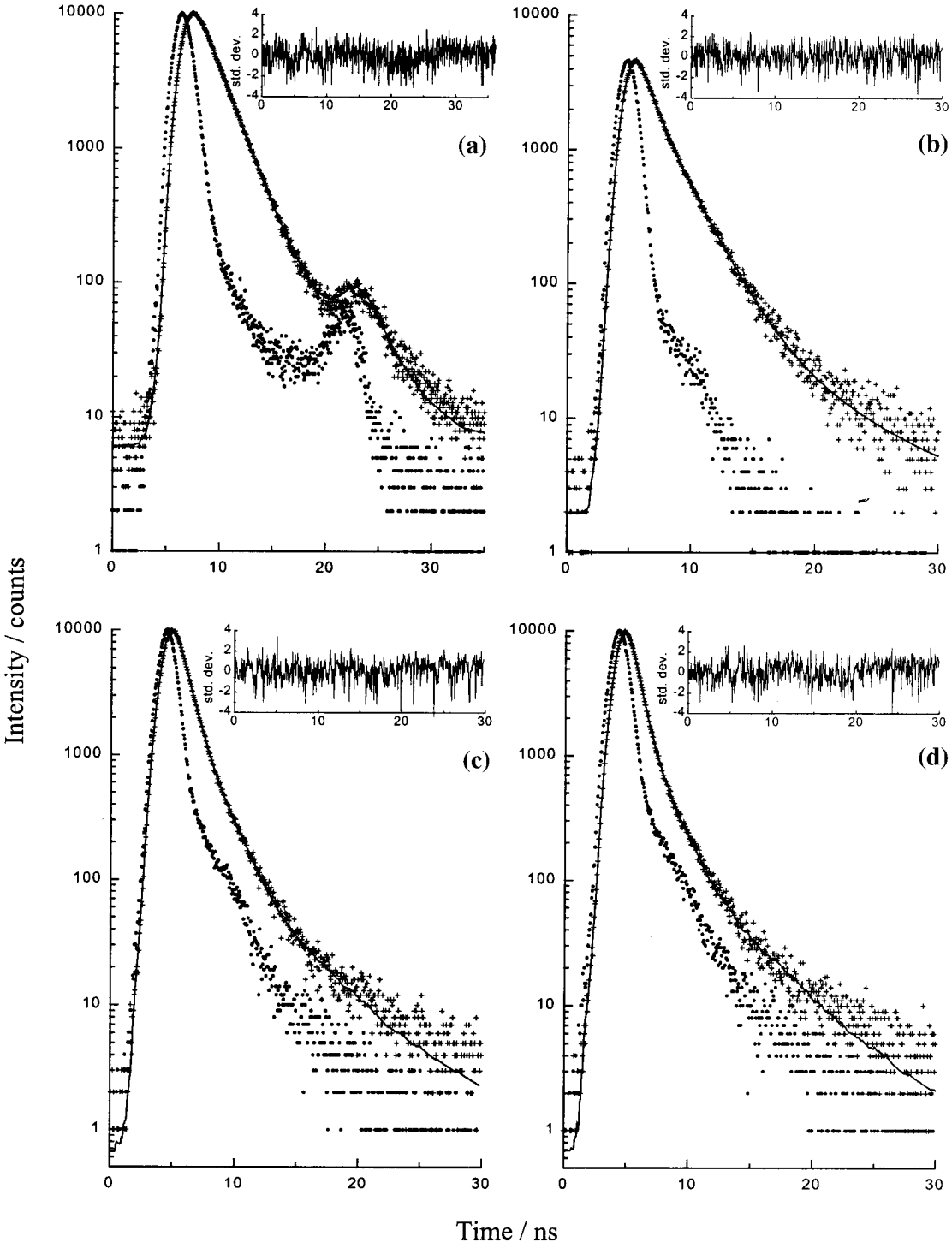

Figure 10. Fluorescence decay data, showing the lamp profile, the sample decay, and the best fit for (a) ZnP/MeOH, (b) ZnP−TiO_2(sp), (c) ZnP−PVP/glass, and (d) ZnP−PVP/TiO_2(sp).

al.[39] Further studies on the time-resolved absorption spectroscopy of these hybrid systems should be pursued to elucidate this matter.

Figure 11 shows the emission spectra from ZnP−PVP/glass and ZnP−PVP/TiO_2(sp) thin films. Emission spectra from ZnP and ZnP−PVP in methanol are also shown in this figure.

Emission from ZnP−PVP/glass, spectrum 1, shows the presence of four bands in the 600−720 nm region. The global fluorescence quantum yield is found to be 0.090, a value higher than ZnP in methanol, as would be expected for a more rigid chromophore. The fluorescence decay obtained from this film and shown in Figure 10c could be fitted to a sum of two dominant contributions $\tau_1 = 0.60$ ns and $\tau_2 = 1.08$ ns, as shown in Table 2, and a third minor component, $\tau_3 = 6.05$ ns, with preexponential factors of 0.57, 0.42, and 0.01, respectively. Decomposition of the ZnP−PVP/glass spectrum, shown in Figure 12, reveals the presence of two distinct spectra, the first one with emission bands located at 612.5 and 668.0 nm and $I(F)_{Q_\alpha}/I(F)_{Q_\beta} = 0.70$. The second spectrum has two bands at 645.0 and 706.4 nm with $I(F)_{Q_\alpha}/I(F)_{Q_\beta} = 2.0$. In view of these data we consider that excited bound ZnP, (ZnP−PVP)* molecules, can probe two distinct microenvironments within the polymer matrix, most probably the faster component in the fluorescence decay originates from ZnP molecules embedded

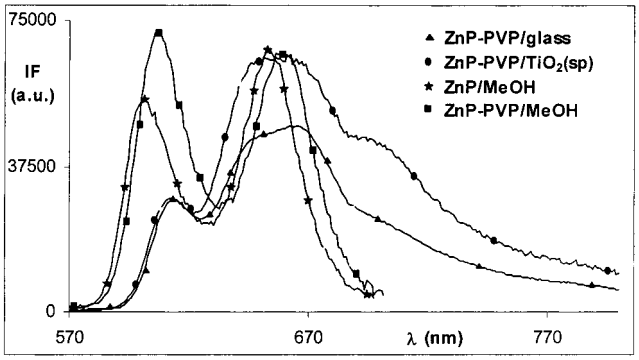

Figure 11. Emission spectra from ZnP−PVP/glass and ZnP−PVP−TiO_2(sp) thin films and from ZnP and ZnP−PVP in methanol.

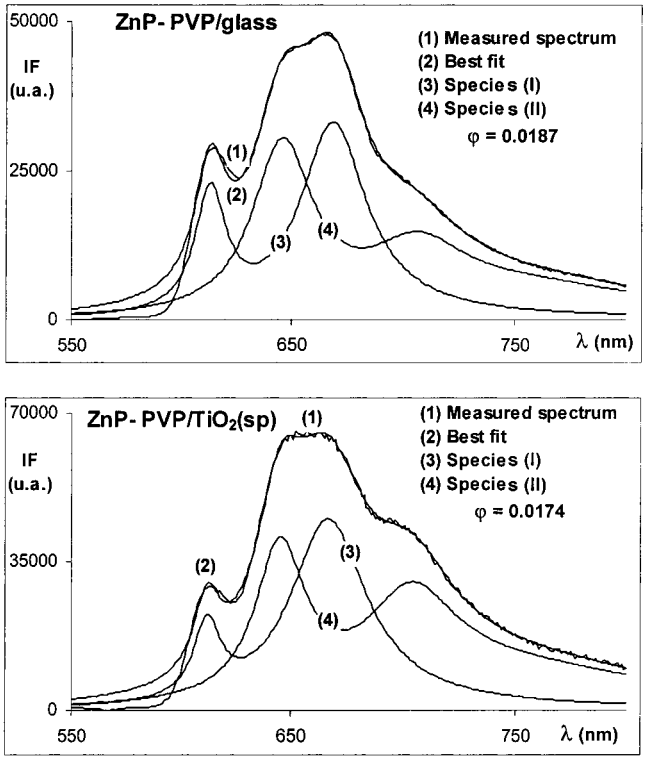

Figure 12. Measured and calculated fluorescence spectra of ZnP−PVP/glass and ZnP−PVP/TiO_2(sp). It is possible to distinguish two emissions ascribed to different micropolarities of the copolymer.

in regions of higher polarity whereas the longer lived emission originates from (ZnP−PVP)* in a less polar microenvironment.[40] We therefore ascribe the emission from 612.5 and 668.0 nm bands to the longer lived species that probe the less polar environment and the second spectrum to the short-lived species originating from (ZnP−PVP)* that probe the more polar environment within the copolymer matrix. In fact, the styrene units possess a much lower dielectric constant than pyridine units. This feature is corroborated upon comparison of ZnP−PVP/glass spectrum of Figure 11 with the emission measured from ZnP−PVP/MeOH, shown in the same figure, where only two bands at 607.5 and 659.5 nm can be found, with $I(F)_{Q_\alpha}/I(F)_{Q_\beta} = 1.08$. In this latter situation we admit that only one type of solvent relaxation regime is found. These results are also shown in Table 2. This is to be expected since now the polymeric chains are embedded in methanol. However, the occurrence of specific interactions between (ZnP−PVP)* and the polymeric chain and/or (ZnP−PVP)* and ZnP−PVP can also be anticipated, although further studies are needed to elucidate unambiguously the nature of the second emission.

The steady-state emission of ZnP−PVP/TiO_2(sp), also shown in Figure 11, displays the same features as ZnP−PVP/glass (see Figure 12 and Table 2), as would be expected since most of ZnP is bound to PVP on the top layer of this system as previously described in section 4.1. The band centered at 665.8 nm becomes slightly more prominent in this spectrum as compared with the ZnP−PVP/glass system. This feature is in agreement with the presence of a small fraction of ZnP incorporated into the titania matrix, as reported in 4.1.

Table 2 summarizes all data obtained from the emission studies on the films and also some relevant data from studies in methanolic solutions.

5. Conclusion

In the present work we have measured the extinction coefficient, $k(E)$, and the refractive index, $n(E)$, of ZnP when incorporated into titania, by a method that takes into account the nanoporous structure of TiO_2 matrixes prepared by sol−gel and reactive sputtering techniques. Both optical absorption and photoluminescence data show that a specific interaction occurs between the zinc atom of the porphyrin and donor groups on the surface of titania, whereby the porphyrin becomes "anchored" onto the surface of the semiconductor either in the form of isolated molecules or in the form of aggregates. Moreover, the adopted methodology enabled the authors to distinguish in the absorption and in the emission spectra the contributions from the monomer and the aggregates. This provided an accurate means of obtaining the fluorescence quantum yield and lifetimes of both forms.

Also included in this work are the absorption and emission studies of ZnP bound to poly(4-vinylpyridine) (PVP). In this case no ground-state interaction between porphyrin molecules could be detected due to the formation of a complex between ZnP and PVP. This complex is fluorescent with two distinct radiative decays determined by the dual polarity of the host copolymer.

High absorption coefficients for the 400−700 nm region of the electromagnetic spectrum can be attained with both ZnP−PVP and ZnP−TiO_2 systems produced under the experimental conditions used in this work. This is a promising feature regarding the potential application of these hybrid systems in liquid-junction solar cells.

Acknowledgment. We gratefully acknowledge Mr. M. R. Pereira's contribution in the preparation of the sol-gel-derived titania film.

References and Notes

(1) O'Reagan, B.; Grätzel, M. *Nature* **1991**, *353*, 737.

(2) *Book of Abstracts of the 13th International Conference on Photochemical Conversion and Storage of Solar Energy*, Snowmass, Colorado, U.S.A., July, 2000; (see also references therein).

(3) Shang-Di Mo; Ching, W. Y. *Phys. Rev. B* **1995**, *51*, 13 023.

(4) Tachibana, Y.; Haque, S. A.; Mercer, I. P.; Durrant, J. R.; Klug, D. R. *J. Phys. Chem. B* **2000**, *104*, 1198.

(5) Koehorst, R. B. M.; Boschloo, G. K.; Savanije, T. J.; Goossens, A.; Shaafsma, T. J. *J. Phys. Chem. B* **2000**, *104*, 2371.

(6) Cahen, D.; Hodes, G.; Grätzel, M.; Guillemoles, J. F.; Riess, I. *J. Phys. Chem. B* **2000**, *104*, 2053.

(7) Kalyanasundaram, K.; Grätzel, M. *Coord. Chem. Rev.* **1998**, *77*, 347.

(8) Darwent, J. R.; Douglas, P.; Harriman, A.; Porter, G.; Richoux, M.-C. *Coord. Chem. Rev.* **1982**, *44*, 83.

(9) Kalyanasundaram, K.; Vlachopoulos, N.; Krishnan, V.; Monnier, A.; Grätzel, M. *J. Phys. Chem.* **1987**, *91*, 2342.

(10) Mao, H.; Deng, H.; Li, H.; Shen, Y.; Lu, Z.; Xu, H. *J. Photochem. Photobiol. A: Chem.* **1998**, *114*, 209.

(11) Hungerford, G.; Ferreira, M. I. C.; Pereira, M. R.; Ferreira, J. F. A.; Coelho, A. F. *J. Fluorescence* **2000**, *10*, 283.
(12) Fuqua, P. D.; Dunn, B.; Zink, J. I. *J. Sol-Gel Sci. Technol.* **1998**, *11*, 241.
(13) Viseu, T. M. R.; Ferreira, M. I. C. *Vacuum* **1999**, *52*, 115.
(14) Reisfeld, R. *J. Non-Cryst. Solids* **1990**, *121*, 254.
(15) Demas, J. N.; Crosby, G. A. *J. Phys. Chem*. **1971**, *75*, 991.
(16) Langford, J. I. *J. Appl. Crystallogr*. **1978**, *11*, 10.
(17) Viseu, T. M. R.; Almeida, B.; Stchakovsky, M.; Drevillon, B.; Ferreira, M. I. C.; Sousa, J. B. Accepted for publication in *Thin Solid Films*.
(18) Scheidt, W. R. In *The Porphyrins*; Dolphin, D., Ed.; Academic Press, Inc.: New York, 1978; Vol. III, Chapter 10.
(19) Abelès, F. In *Optics of Thin Films—Advanced Optical Techniques*; Van Heel, A. C. S., Ed.; North-Holland: Amsterdam, 1967; Chapter V.
(20) Forhoui, A. R.; Bloomer, I. *Phys. Rev. B* **1986**, *34*, 7018.
(21) Webman, I.; Jortner, J.; Cohen, M. H. *Phys. Rev. B* **1977**, *15*, 5712.
(22) Bohren, C. F.; Huffman, D. R. *Absorption and Scattering of Light by Small Particles*; Wiley: New York, 1998.
(23) Sakurai, J. J. *Advanced Quantum Mechanics*; Addison-Wesley: Reading, MA, 1967.
(24) Heitler, W. *The Quantum Theory of Radiation*; Dover: New York, 1984.
(25) Nappa, M.; Valentine J. S. *J. Am. Chem. Soc.* **1978**, *100*, 5075.
(26) Ohno, O.; Kaizu, Y.; Kobayashi, H. *J. Chem. Phys*. **1985**, *82*, 1779.
(27) Kirksey, C. H.; Hambright, P.; Storm, C. B. *Inorg. Chem*. **1969**, *8*, 2141.
(28) Kumar, P. M.; Badrinarayanan, S.; Sastry, M. *Thin Solid Films* **2000**, *358*, 122.
(29) Khairutdinov, R. F.; Serpone, N. *J. Phys. Chem*. **1995**, *99*, 11952.
(30) Kemnitz, K.; Tamai, N.; Yamakasi, I.; Nakashima, N.; Yoshihara, K. *J. Phys. Chem.* **1986**, *90*, 5094.
(31) Scott, D.; Hayes, R. G. *Inorg. Chem.* **1983**, *22*, 3050.
(32) Previous work by some of the authors has shown the formation of a ground-state complex between ZnTPP and PVP, in methanol, with an equilibrium constant of 88 M^{-1}.
(33) Vogel, G. C.; Stahlbush, J. R. *Inorg. Chem*. **1977**, *16*, 950.
(34) Cruz, F.; Driaf, K.; Berthier, C.; Lameille, J.-M.; Armand, F. *Thin Solid Films* **1999**, *349*, 155.
(35) McRae, E. G.; Kasha, M. *J. Chem. Phys.* **1958**, *28*, 721.
(36) Hochstrasser, R. M.; Kasha, M. *Photochem. Photobiol*. **1964**, *3*, 317.
(37) Kasha, M.; Rawls, H. R.; El-Bayoumi, M. A. *Pure Appl. Chem*. **1965**, *11*, 371.
(38) Durrant, J. R.; Tachibana, Y.; Mercer, I.; Moser, J. E.; Grätzel, M.; Klug, D. R. *Z. Phys. Chem.* **1999**, *212* (1), 93.
(39) Burfeindt, B.; Zimmermann, C.; Ramakrishna, S.; Hannappel, T.; Meissner, B.; Storck, W.; Willig, F. *Z. Phys. Chem.* **1999**, *212* (1), 67.
(40) The emission spectrum of species I from ZnP−PVP/glass or ZnP−PVP/TiO_2(sp), shown in Figure 12, is quite similar to the emission observed from ZnP in solvents of low polarity, in that $I(F)_{Q_\alpha}/I(F)_{Q_\beta} < 1$, whereas emission of species II tends to the emission pattern observed in polar solvents such as DMSO, DMF and CH3CN, where the same ratio $I(F)_{Q_\alpha}/I(F)_{Q_\beta} \geq 1$.